Electronic Supplementary Material (ESI) for RSC Advances.

Analysis of electron transfer dynamics in mixed community electroactive microbial biofilms

Bernardino Virdis, Diego Millo, Bogdan C. Donose, Yang Lu, Damien J. Batstone, Jens O. Krömer

Supplementary information

Content:

Figure S1. Spectroelectrochemical cell

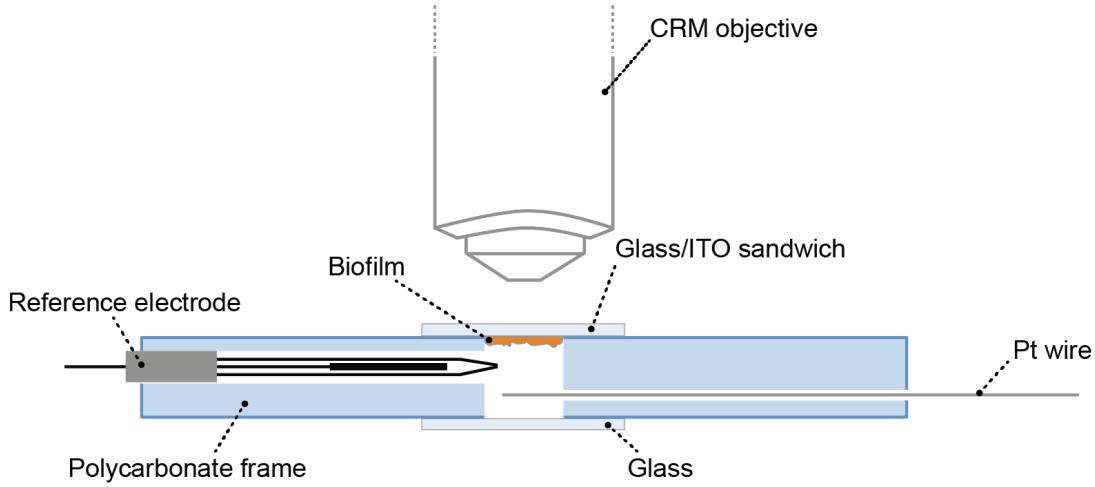

Figure S1. Schematic representation of the electrochemical cell used for the confocal resonance Raman microscopy observations. The glass/ITO sandwich served as working electrode with total area of 1 cm^2. The Pt wire served as counter electrode. The total internal volume was 1 mL. Image not to scale.

Figure S2. Effect of laser power on the intensity of the Raman scattering

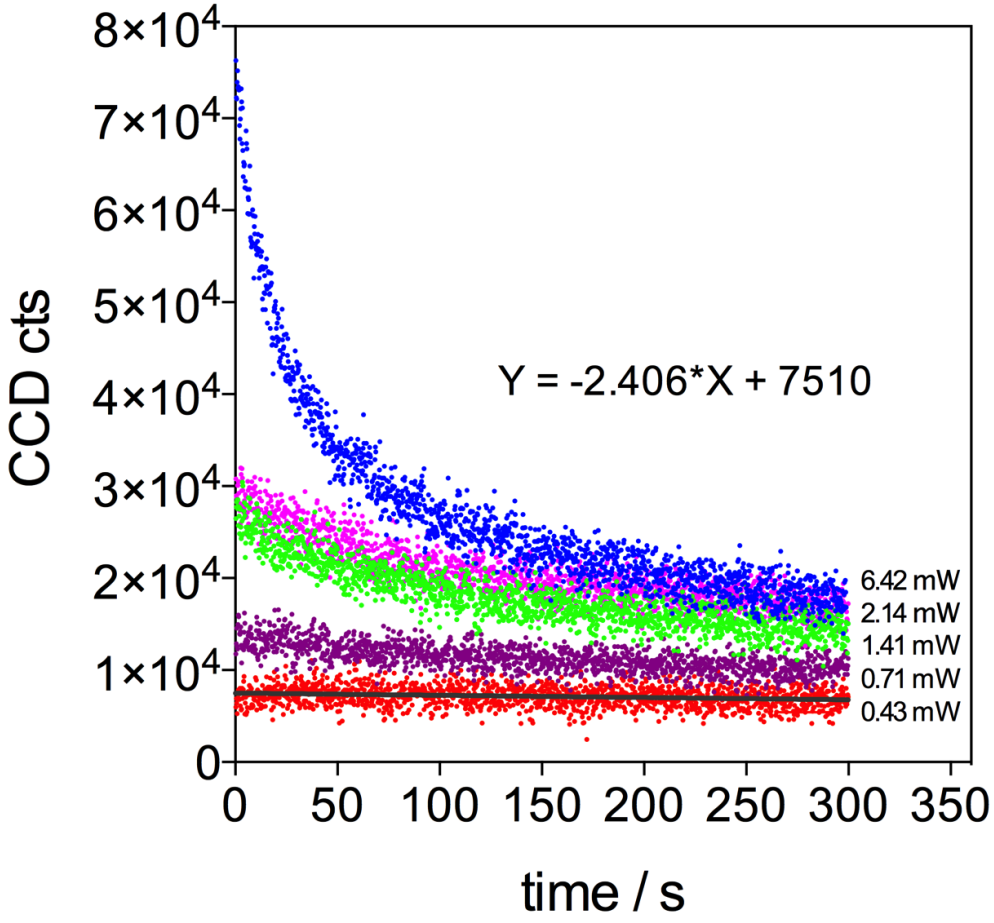

Figure S2. Effect of laser power on the stability of the intensity of the Raman scattering of the mode ν_{15} ($I\nu_{15}$) at 750 cm^{-1}. RR spectra collected continuously using different power of the laser line at 532 nm and with an accumulation time of 0.2 s. At the lowest power of 0.43 mW $I\nu_{15}$ dropped of <10% in 300 seconds. At powers lower than 0.43 mW, the peaks in the RR spectra were not resolvable.

Text S1. Determination of the electrode/biofilm interface location and depth profiling

The confocal capabilities of the system were characterized by collecting intensity profile *vs* depth signals using a 500 µm thick glass slide placed on top of a polished silicon wafer. Data in Figure S3 represents integrated intensity (microcrystalline Si Raman band, 520 cm^{-1}) dependence on nominal depth, were scale was zeroed at the outer surface of the glass. This configuration offers a punctual response since silicon is a strong absorbent of the green laser and allows the determination of the instrumental Point Spread Function profile.[1] Having the correction collar set at 500 μm and a depth compression factor of 1.5 (refractive index aberration) the analysis of the Lorentzian fit of the intensity profile leads to an estimated depth resolution of 14.2 µm. This approach allows establishing the location of glass interface at 342 um below the focal point of the glass surface (Figure S3) corresponding to the maximum in the Si Raman band. Further on, the interface location was used as reference when designing the depth profile experiments for each biofilm RR spectra collected. An example of this measurement is shown in Figure S4. Typically, spectral acquisition on biofilm sections (depth measurements) was done using integration times of 20 s/point, which was sufficient to obtain high-contrast resonance spectra in 12 points over 60 μm. The vertical coordinates of the spectral data were assigned to a particular location during data processing. The data from different locations were then grouped per 5 μm intervals (Table S1 and S2) and were used to reconstruct the profiles shown in Figure 3 in the manuscript.

Figure S3. Variation of the intensity of the Raman scattering of silicon binned at the band 520 cm^{-1} in the Z-direction

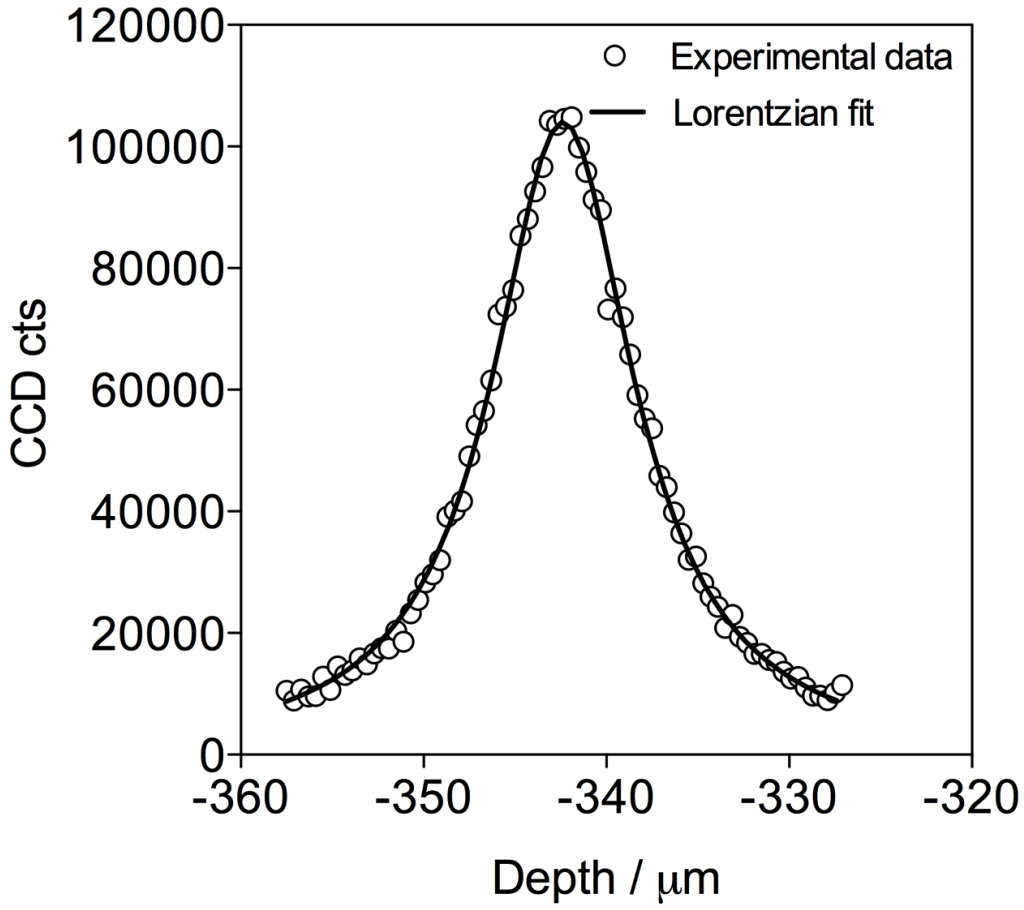

Figure S3. Integrated intensity profile for the Silicon band (520 cm^{-1}) vs. nominal depth used to locate the electrode interface and depth resolution. The measurement was performed using a silicon wafer covered by a 500 μm thick glass slide. The glass-silicon interface is found at 342 μm below the air-glass interface focal point (assumed as zero).

Figure S4. Depth profiling: RR spectra of biofilms collected along the Z-direction

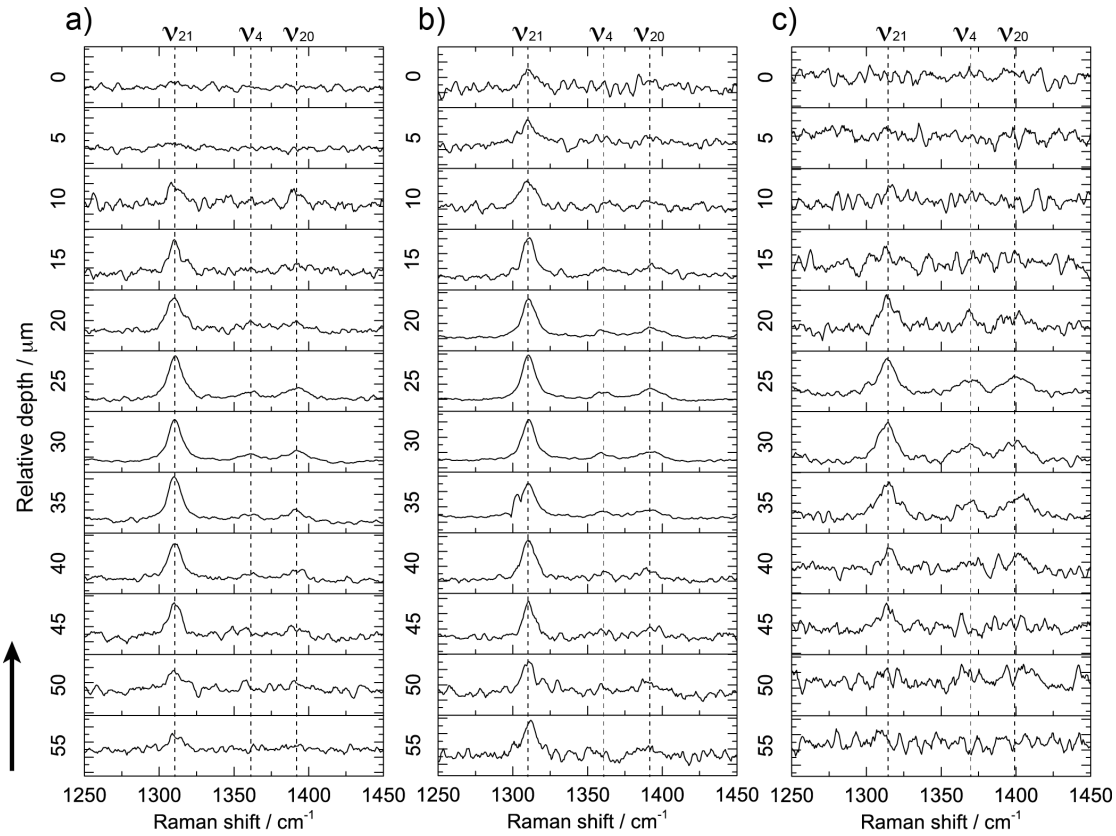

Figure S4. Example of depth profiling measurements with the working electrode poised at +0.2 V vs. Ag/AgCl, in the presence of a) 20 mM, b) 5 mM, and c) 1 mM acetate. Each RR spectrum was collected using a 20 s acquisition time and the profile is composed of 12 spectra recorded along a 60 μm line every 5 μm. Not that the zero coordinate represents the end of the depth scan and not the electrode-biofilm interface. The arrow indicates the direction of scan. The Raman shift position of the bands ν_{21}, ν_4, and ν_{20} was determined by Lorenzian fitting of the RR spectra within the region between 1250 and 1450 cm^{-1} (average results for all measurements are summarised in Table S1 and S2 for the test at 0 V and +0.2 V, respectively).

Table S1. Depth profiling: relative position of redox marker bands ν_{21}, ν_4, ν_{20} under potentiostatic control with E_{anode} at 0 V

Table S1. Relative position of redox marker bands ν_{21}, ν_4, ν_{20} as a function of the distance from the ITO interface at various acetate concentrations. The anode electrode was poised at 0 V *vs* Ag/AgCl. Values are reported as averages ± standard deviations for triplicate measurements.

E_{anode}: 0 V vs. Ag/AgCl			
Depth (μm)	ν_{21} (cm^{-1})	ν_4 (cm^{-1})	ν_{20} (cm^{-1})
0-5	1310.5±0.2	1360.3±0.5	1392.3±0.4
5-10	1310.5±0.2	1359.6±0.3	1392.4±0.4
10-15	1310.4±0.4	1359.5±0.4	1392.0±0.7
15-20	1310.3±0.2	1360.2±0.9	1391.9±1.4
20 mM Acetate			
0-5	1310.6±0.4	1360.1±0.9	1391.9±0.2
5-10	1310.5±0.4	1359.5±0.2	1391.9±0.2
10-15	1310.5±0.4	1360.3±1.6	1391.6±0.4
15-20	1310.5±0.2	1359.2±0.6	1391.1±1.0
5 mM Acetate			
0-5	1313.0±0.8	1367.2±1.7	1399.8±2.8
5-10	1312.7±1.1	1367.3±2.6	1398.9±2.7
10-15	1313.4±0.5	1368.2±0.05	1401.3±0.8
15-20	1313.2±0.1	1368.8±0.1	1401.0±0.4
1 mM Acetate			

Table S2. Depth profiling: relative position of redox marker bands ν_{21}, ν_4, ν_{20} under potentiostatic control with E_{anode} at +0.2 V

Table S2. Relative position of redox marker bands ν_{21}, ν_4, ν_{20} as a function of the distance from the ITO interface at various acetate concentrations. The anode electrode was poised at +0.2 V vs. Ag/AgCl. Values are reported as average ± standard deviations for triplicate measurements.

E_{anode}: +0.2 V vs. Ag/AgCl			
Depth (μm)	ν_{21} (cm^{-1})	ν_4 (cm^{-1})	ν_{20} (cm^{-1})
0-5	1310.7±0.1	1360.0±0.4	1392.0±0.3
5-10	1310.5±0.1	1360.7±1.0	1391.7±0.5
10-15	1310.4±0.2	1360.1±0.8	1391.5±0.1
15-20	1310.4±0.5	1359.5±0.4	1391.3±0.8
20 mM Acetate			
0-5	1310.5±0.2	1359.6±0.8	1392.1±0.6
5-10	1310.5±0.3	1359.1±1.2	1392.1±0.8
10-15	1310.5±0.3	1359.1±0.5	1391.4±0.5
15-20	-	-	-
5 mM Acetate			
0-5	1313.8±0.6	1368.1±0.8	1400.5±0.6
5-10	1313.5±0.5	1367.7±1.0	1400.3±0.8
10-15	1313.5±0.1	1368.7±0.8	1400.7±0.6
15-20	1313.4±0.7	1368.7±0.2	1402.3±0.9
1 mM Acetate			

Text S2. Fluorescent *in situ* Hybridization (FISH) and COMSTAT analysis

Biofilms were removed from 3 representative electrochemical cells and fixed for 2 hours with 4% paraformaldehyde as a whole and scratched off samples and then washed with phosphate buffered saline solution (130 mM sodium chloride, 10 mM sodium phosphate buffer, pH 7.2). The samples were then dehydrated for 3 minutes in ethanol series 50%, 70% and 98% respectively. After drying, FISH was performed directly on the biofilms as described by.[2] Details of oligonucleotide FISH probes are listed in Table S3. The slides were viewed under Zeiss Axioscope LSM510 confocal microscope (Zeiss, USA). Z-stack images (n > 30, with 1 μm interval) were taken directly from each biofilm. The biofilm structure was analysed using COMSTAT image analysis software, using connected volume filtration to reduce background noise.[3] Biofilm thickness on the three replicates was determined as (17±4) μm (average ± standard deviation). Relative abundance of *Geobacter* was quantified as (54.4±15.2) % (standard deviation ± 95% congruency) from scratched off biofilm images (n = 13) using DAIME image analysis software.[4] This is in good agreement with 16S rRNA amplicon sequencing results (data not shown).

Table S3. List of FISH probes used for biofilm characterization.

Target population(s)	**FISH probe fluorochrome**	**Probe sequences(5'-3')**	**References**
Bacteria	*EUB338-FITC*	GCT GCC TCC CGT AGG AGT	Amann *et al.*[5]
	EUB338II-FITC	GCA GCC ACC CGT AGG TGT	Daims *et al.*[6]
	EUB338III-FITC	GCT GCC ACC CGT AGG TGT	Daims *et al.*[6]
Geobacter	*GEO1a-Cy3*	CTC ACG CAC TTC GGG ACC AG	Demanèche *et al.*[7]
	GEO1b-Cy3	CTC ACG CAC TTC GGG ACC AA	Demanèche *et al.*[7]

Figure S5. CLSM and FISH micrographs

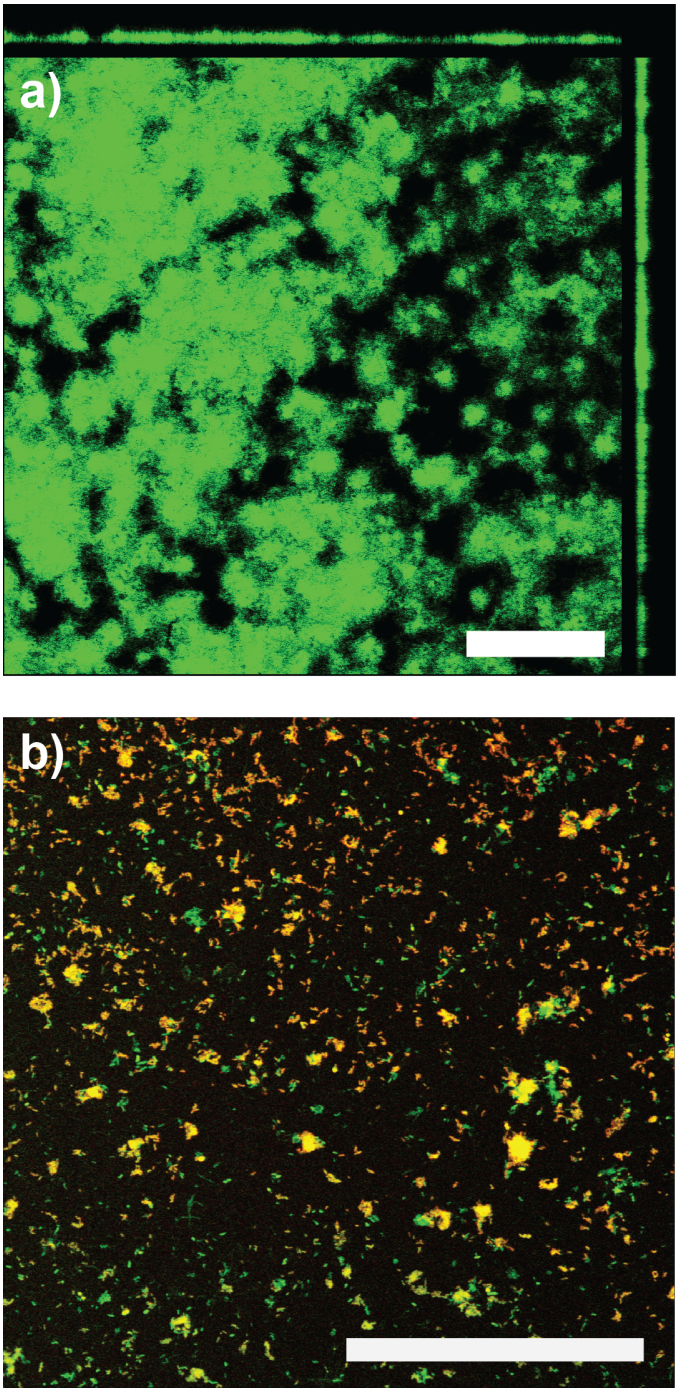

Figure S5. Representative FISH micrograph of fully-developed biofilm on an ITO electrode detecting all bacteria (*EUBmix*) in green from Z-stack scan (a). Top and lateral inserts in are representative orthogonal slices of the biofilm perpendicular to the ITO surface. (b) Representative FISH micrograph in scratched off biofilms under higher magnification, detecting *Geobacter* (*GEOmix*) in yellow and other bacteria in green. Scale bars equals to 100 µm.

Figure S6. Average catalytic current generation by electroactive biofilms at different levels of substrate and different anodic electrode potentials

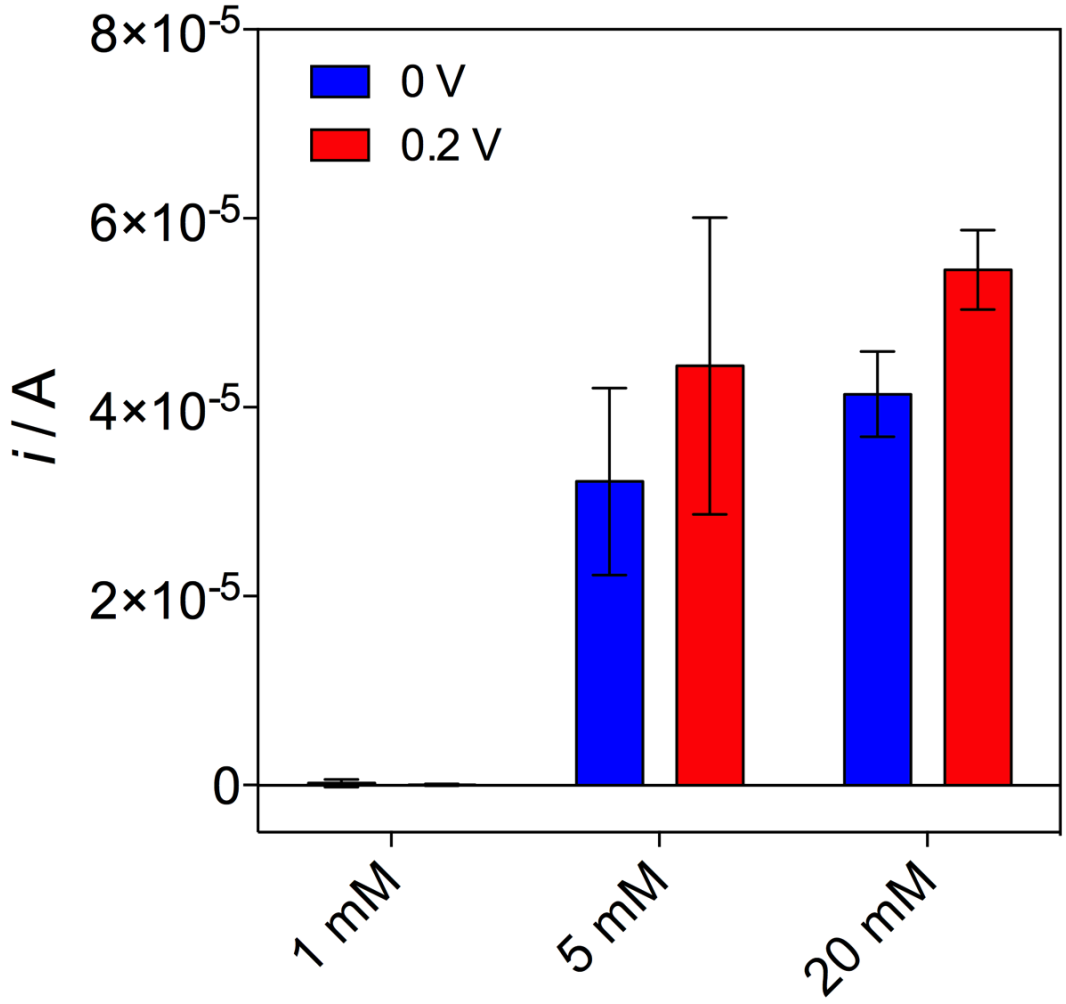

Figure S6. Average (± standard deviations) current production by electroactive biofilms during potentiostatic operations, as a function of the concentration of acetate.

Figure S7. CRRM and CA measurements for potential transitions with E_i = -0.5 V to E_f = 0 V

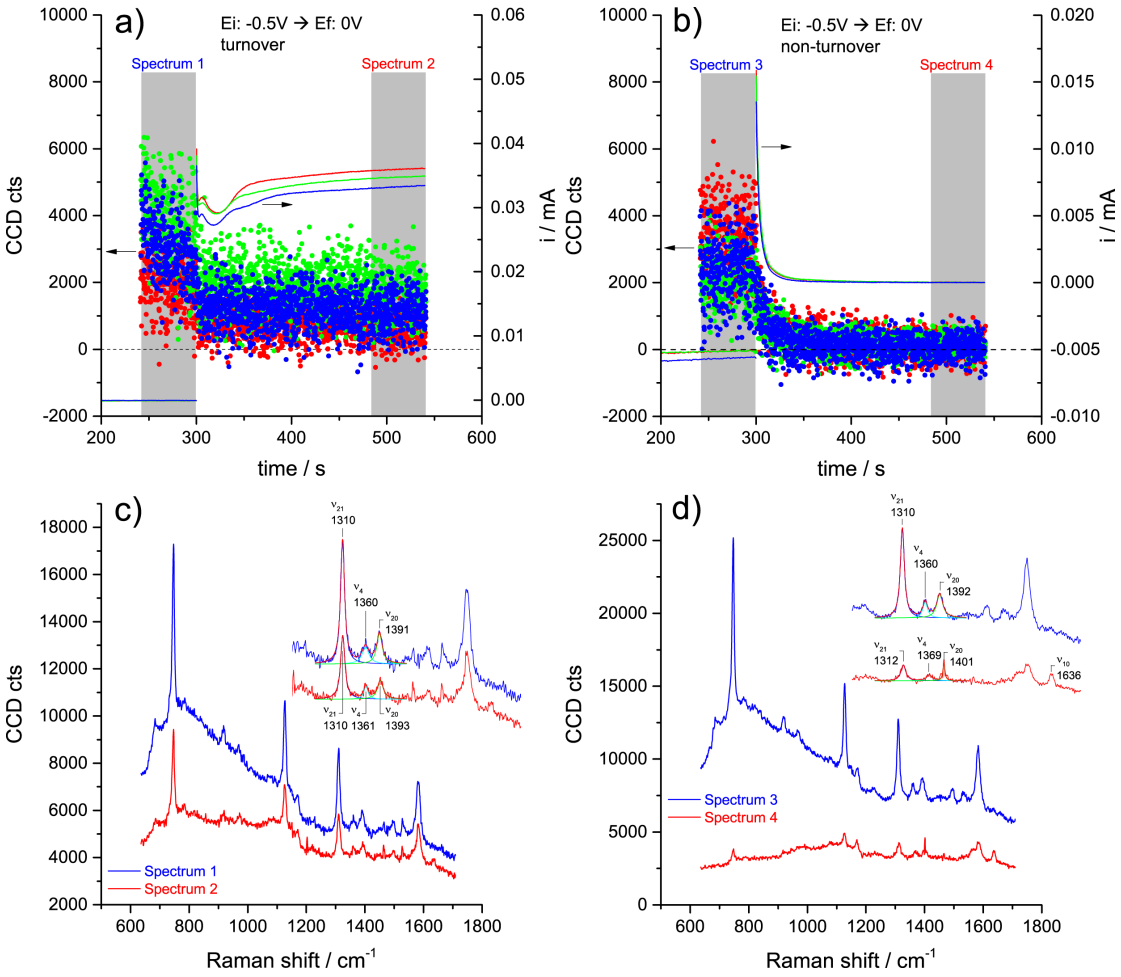

Figure S7. CRRM and CA measurements for potential steps with E_i = -0.5 V to E_f = 0 V. (a) Current *vs* time and intensity of the band ν_{15} vs time during the test under turnover and (b) non-turnover conditions. (c and d) RR spectra recorded during a 60 s accumulation before the transition (spectra 1 and 3) and again 180 s after the transition (spectra 2 and 4) during (c) turnover and (d) non-turnover measurements. Inserts in (c) and (d) represent magnification on the redox markers region and shows relative position of the bands ν_{21}, ν_4, ν_{20}, and ν_{10}.

Figure S8. Dependency of the electron transfer rate constant for homogeneous electron transfer (k^0_{hom}) with the overpotential

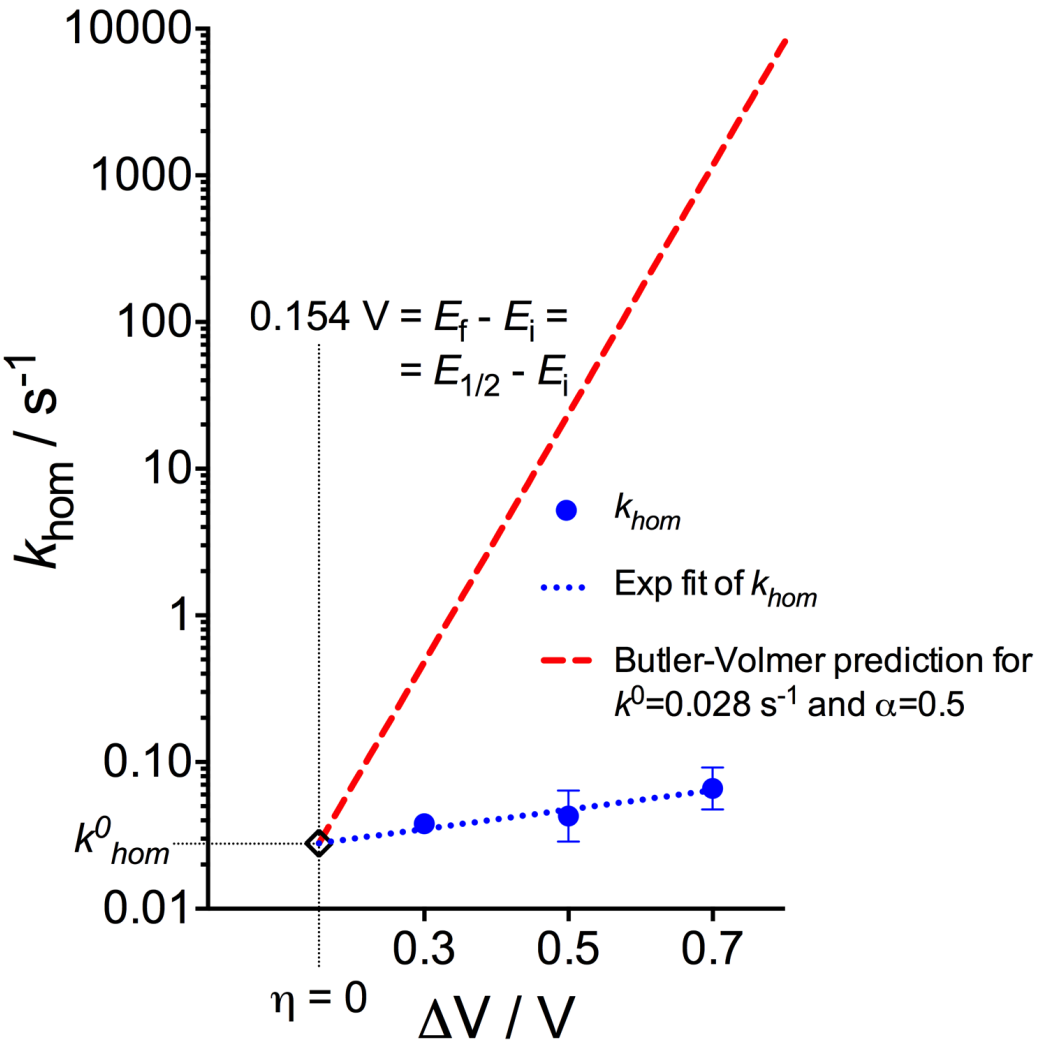

Figure S8. Non-linear fit of k_{hom} values and estimation of the ET rate constant k^0 for the ideal potential transition with zero overpotential, that is from E_i = -0.5 V to E_f = $E_{1/2}$ = -0.346 V (where $E_{1/2}$ is the arithmetic average is the two redox couples as evidenced by nonturnover voltammetry (Figure 1 in the Manuscript)). Using the so-determined k^0, k_{hom} can be modeled using the Butler-Volmer formalism:[8]

$$k_{hom}^{BV} = k_{hom}^{0} \exp\left(\frac{(1-\alpha)nF}{RT}\left(E - E_{1/2}\right)\right)$$

where for n = 1 T = 298 K, R = 8.31 J mol^{-1} K^{-1}, F = 96485 C mol^{-1}, and for a relevant value of the symmetry coefficient (α = 0.5).

Text S3. Supplementary References

1 M. de L. P. Miguel and J. P. Tomba, *Progress in Organic Coatings*, 2012, **74**, 43–49.

2 R. Amann, J. Snaidr, M. Wagner, W. Ludwig and K. H. Schleifer, *J Bacteriol*, 1996, **178**, 3496–3500.

3 A. Heydorn, A. T. Nielsen, M. Hentzer, C. Sternberg, M. Givskov, B. K. Ersbøll and S. Molin, *Microbiology (Reading, Engl)*, 2000, **146 (Pt 10)**, 2395–2407.

4 H. Daims, S. Lücker and M. Wagner, *Environ Microbiol*, 2006, **8**, 200–213.

5 R. I. Amann, B. J. Binder, R. J. Olson, S. W. Chisholm, R. Devereux and D. A. Stahl, *Appl Environ Microbiol*, 1990, **56**, 1919–1925.

6 H. Daims, A. Brühl, R. Amann, K. H. Schleifer and M. Wagner, *Systematic and Applied Microbiology*, 1999, **22**, 434–444.

7 S. Demanèche, H. Sanguin, J. Poté, E. Navarro, D. Bernillon, P. Mavingui, W. Wildi, T. M. Vogel and P. Simonet, *Proceedings of the National Academy of Sciences*, 2008, **105**, 3957–3962.

8 A. J. Bard and L. R. Faulkner, *Electrochemical Methods*, Wiley, 2000.